Asian Journal of Chemistry; Vol. 37, No. 12 (2025), 3167-3176
ASIAN JOURNAL OF CHEMISTRY
https://doi.org/10.14233/ajchem.2025.34891

Sustainable Fabrication of Magnetic Biochar from Corncob Waste for Efficient Removal of Indigo Carmine from Textile Effluent

KOFFI PIERRE DIT ADAMA N'GORAN[1,*], NAMINATA SANGARE[2], KAKOU CHARLES KINIMO[1], N'GUESSAN LOUIS BERENGER KOUASSI[1], LEMEYONOUIN ALIOU GUILLAUME POHAN[2], DONOUROU DIABATE[2], KOFFI MARCELLIN YAO[3] and ALBERT TROKOUREY[2]

[1]Département de Mathématiques Physique Chimie, Université Peleforo GON COULIBALY, BP 1328 Korhogo, Côte d'Ivoire
[2]Laboratoire de Chimie Physique, Université Félix Houphouët-Boigny, 22 BP 582 Abidjan 22, Côte d'Ivoire
[3]Centre de Recherches Océanologiques, Département Environnement, 29 rue des Pêcheurs, BP V 18 Abidjan, Côte d'Ivoire

*Corresponding author: E-mail: ngorankoffipierre@gmail.com

Received: 14 September 2025 *Accepted*: 17 November 2025 *Published online*: 30 November 2025 AJC-22208

This work aimed to remove indigo carmine from water using an iron oxide–corncob biochar (α-Fe_2O_3-C) composite synthesized hydrothermally and characterized by SEM, XRD, FTIR and TGA techniques. The composite averaging 20.63 nm, contained carboxylic, hydroxyl, phenolic and alcoholic groups. Adsorption analysis showed higher efficiencies for α-Fe_2O_3-C than for raw biochar in both aqueous solutions (88.58-96.66% *versus* 71.94-79.93%) and real effluent (48.01-61.90% *versus* 31.74-43.66%). The Langmuir model best described adsorption on biochar, while the Freundlich model fitted the best for the magnetic based biochar composite. Maximum capacities (Q_{max}) were 4.76 mg/g (biochar) and 12.72 mg/g (α-Fe_2O_3-C). Overall, the composite significantly improved indigo carmine removal and shows potential for treating dye-contaminated industrial effluents.

Keywords: Iron oxide, Corncob biochar, Indigo carmine, Adsorption, Textile effluent.

INTRODUCTION

Since the early 2000s, the rapid expansion of the dye industry has led to the rampant release of large quantities of untreated dye-laden wastewater into the environment particularly in the under developed countries. This discharge poses a significant threat to aquatic ecosystems and public health. Several dyes are resistant to biodegradation and are known to exhibit toxic and carcinogenic properties, making their presence in water bodies particularly hazardous [1]. The presence of organic dyes in water, even at very low concentrations, reduces light penetration and negatively impacts plant photosynthesis, affecting their growth and all aquatic life [1-3]. Therefore, the presence of dyes in water warrants particular attention due to their potential environmental and health impacts.

Indigo carmine, an organic dye, is widely used across the textile, cosmetics, pharmaceutical and food industries and is frequently released into the environment [4]. Human ingestion of indigo carmine (above 5 mg/kg) can cause gastrointestinal, cardiovascular and hypertension disorders [5]. It is, therefore, necessary to remove indigo carmine from effluents before releasing them into the environment. Several water purification methods and techniques, such as membrane processes, oxidation and adsorption, have been developed to treat water contaminated by chemical pollutants [6-8]. Adsorption, a widely used and simple technique employing various adsorbents such as carbon, often faces challenges in separating the carbon from treated effluents, a limitation effectively addressed by incorporating magnetic materials [9,10].

Iron oxide nanoparticles are increasingly used in water treatment because of their good magnetic properties, enabling them to be easily removed from solution [11-14]. The encapsulation of carbon within magnetic particles enables efficient separation and recovery of spent carbon using a magnetic field. In addition, iron oxide-based composites are likely to improve pollutant adsorption [15-18]. For example, the removal of methylene blue from aqueous solutions was enhanced by Fe_2O_3@carbon peanut shell [16] and Fe_3O_4-carbon sorghum straw composites [17], while the Fe_3O_4-Ag-carbon palm kernel

hull composite improved the adsorption of cadmium and lead [18] and the Fe_3O_4-graphene oxide-grape fruit peel carbon composite increased the uptake of ciprofloxacin in aqueous solution [19].

Corn cobs are a source of environmental pollution in developing countries and often disposed of by open burning, which generates carbon dioxide (CO_2), a source of global warming [20,21]. In order to mitigate environmental pollution, it is important to valourize corn cobs as carbon precursors for water treatment and in Côte d'Ivoire, several studies have explored the use of agricultural wastes such as makoré [22], coconut [23], groundnut [24], cashew [25], shea shells [25] and banana peels [26] as precursors for activated carbons. Although various studies have highlighted the adsorption potential of carbons for organic dyes and metallic contaminants, they have seldom considered integration with iron oxides or real-world adsorption kinetics. Thus, the present research emphasizes the combined synergy between carbon adsorption and magnetic filtration and in understanding the kinetics of indigo adsorption in a real environment. Specifically, it focuses on synthesizing and characterizing the corn cob-based composite, investigating the effects of contact time and adsorbent mass on indigo carmine removal in both synthetic and real solutions, examining the influence of initial dye concentration in aqueous solution and modeling the adsorption using Langmuir and Freundlich isotherms.

EXPERIMENTAL

Preparation of corn cob charcoal: Corn cobs were collected from the local village of Korhogo, northern Côte d'Ivoire. The corn cobs were washed thoroughly with distilled water to remove impurities and then oven-dried at 80 ºC for 24 h. The corn cobs were calcined in a muffle furnace for 2 h at 400 ºC to obtain corn cob charcoal [27]. After calcination, the charcoal was ground using an agar mortar and sieved to 100 µm.

Preparation of iron oxide@carbon composite: The composite was synthesized according to the hydrothermal method [28] with slight modifications. In brief, freshly prepared aqueous Fe^{3+} solution was mixed with 5 g of corncob charcoal and then the mixture was stirred with a magnetic stirrer for 30 min at 25 ºC. The resulting suspension was transferred to a 50 mL Teflon-lined hydrothermal reactor, which was heated in a Memmert oven at 150 ºC for 24 h. After hydrothermal treatment, the material was dried in the oven at 80 ºC for 24 h and subsequently calcined at 400 ºC for 2 h and named as α-Fe_2O_3-C.

Characterizations: XRD analysis was carried out at room temperature using a Bruker D8 Advance diffractometer equipped with a copper X-ray source (Cu-*K*α: λ = 1.5405 Å). Acquisitions were made over a 2θ angle range (2θ) varying between 10º and 90º, with a measurement step of 0.02º/s. Infrared analysis was performed with a Thermo-Fisher Scientific Inc. Nicolet 8700 Fourier transform spectrometer, in the range 4000-650 cm^{-1} with a resolution of 5 cm^{-1}. Thermogravimetric analysis (TGA) was performed at a heating rate of 5 ºC min^{-1}. using a TA Instruments TGA Q500 thermogravimetric analyzer (Plate Am). A baseline correction was also performed under a stream of nitrogen, circulating at a flow rate of 20 mL min^{-1}, at the same heating rate with an empty crucible. All analyses were carried out by taking 5 mg of each sample in platinum (Pt) cups at the temperature range 30-900 ºC under air.

Textile effluent sampling: The textile effluent was collected from a gutter in the KOKO district of Korhogo, which receives wastewater from dyeing activities as well as domestic sources.

Adsorption studies: Adsorption experiments were carried out in aqueous solution and in real solution using charcoal and the α-Fe_2O_3-C composite. To 20 mL of each aqueous or real effluent solution containing 5 mg/L of indigo carmine, 0.1 g of carbon or composite was added, which was stirred at 200 rpm using a horizontal stirrer. At regular time intervals (5, 10, 15, 20, 30, 35, 45, 60, 90, 120, 150 and 180 min), aliquots were withdrawn and the suspensions were centrifuged at 5000 rpm for 10 min. The supernatants were then analyzed using a JENWAY UV-visible spectrophotometer at 610 nm. The retention capacity (q_t) of indigo adsorbed and the percentage adsorption at time t were calculated from eqns. 1 and 2, respectively [27]:

$$q_t = \frac{(C_o - C_t) \times V}{m} \quad (1)$$

$$\text{Adsorption } (\%) = \frac{C_o - C_t}{C_o} \times 100 \quad (2)$$

where q_t (mg/g): indigo retention capacity at time t; C_t (mg/L): indigo concentration at time t after adsorption; C_o (mg/L): initial indigo concentration; V (L): volume of initial indigo solution; m (g): mass of material.

Several kinetic models, including pseudo-first-order and pseudo-second-order, are frequently used for adsorption kinetics. The pseudo-first-order model assumes that adsorption is controlled by the formation of bonds between the solute and the active sites [29]. The model is described by the following equation:

$$\frac{dq_t}{dt} = k_1(q_e - q_t) \quad (3)$$

where k_1: the rate constant for pseudo-first-order kinetics; q_t: adsorption capacity at time t; Q_e: adsorption capacity at equilibrium.

Integration of the above eqn. 3 gives:

$$\ln(q_e - q_t) = \ln(q_e) - k_1 t \quad (4)$$

The values of the velocity constant k_1 and the quantity q_e are deduced from the curve.

$$\ln (q_e - q_t) = f(t)$$

The pseudo-second-order model assumes that the adsorption process is governed by chemisorption [30] and is represented by the following formula:

$$\frac{dq_t}{dt} = k_2(q_e - q_t)^2 \quad (5)$$

where k_2 (mg g^{-1} min^{-1}) is the rate constant.

Integration of eqn. 5 gives:

$$\frac{1}{q_t} - \frac{1}{q_e} = \left(\frac{1}{q_e^2 k_2}\right)\frac{1}{t} \quad (6)$$

The constants q_e and k_2 are determined respectively from the y-intercept and the slope of the curve (t/q_t) as a function of t.

Adsorption isotherms: For the experiment on the effect of initial concentration, aqueous indigo solutions with concentrations of 5, 10, 20, 30, 40, and 50 mg/L were prepared. To 20 mL of each solution, 0.1 g of carbon or composite was added. The mixtures were stirred for 2 h at 200 rpm using a horizontal stirrer, then centrifuged at 5,000 rpm for 10 min. The resulting supernatants were analyzed using a JENWAY UV–visible spectrophotometer at 610 nm, and the adsorbed amount (q_e) and percentage removal at equilibrium were calculated according to eqns. 7 and 8, respectively [27]:

$$q_e = \frac{(C_o - C_e) \times V}{m} \quad (7)$$

$$\text{Adsorption } (\%) = \frac{C_o - C_e}{C_o} \times 100 \quad (8)$$

where q_e (mg/g): retention capacity of indigo at equilibrium; C_e (mg/L): residual indigo concentration at equilibrium; C_o (mg/L): initial indigo concentration; V (L): volume of initial indigo solution; m (g): mass of material.

The adsorption of indigo carmine was modeled using the Langmuir and Freundlich isotherms. The Langmuir model is expressed by eqn. 9:

$$q_e = \frac{Q_{max} \times K_L \times C_e}{1 + K_L \times C_e} \quad (9)$$

$$\frac{q_e}{q_m} = \frac{K_L C_e}{1 + K_L C_e} \quad (10)$$

where q_e (mg/g): quantity of substance adsorbed at equilibrium per unit mass of adsorbent, q_m: maximum quantity of substance adsorbed per unit mass of adsorbent (mg/g), C_e: equilibrium adsorbate concentration (mg/L), K_L: Langmuir equilibrium constant (L/g).

Linearization of eqn. 9 leads to the following relationship:

$$\frac{1}{Q_e} = \frac{1}{Q_{max} \times K_L} \times \frac{1}{C_e} + \frac{1}{Q_{max}} \quad (11)$$

By plotting $1/Q_e$ *versus* $1/C_e$, Q_{max} and K_L can be determined.

The Freundlich model is described by eqn. 12:

$$q_e = K_F \times C_e^{1/n} \quad (12)$$

where q_e (mg/g): quantity of solute adsorbed per unit mass of adsorbent at equilibrium; K_F: Freundlich constant for adsorption capacity; n: Freundlich constant for adsorption intensity; C_e (mg/L): adsorbate concentration at equilibrium.

The linear form of the Freundlich equation is as follows:

$$\ln q_e = \ln K_F + \frac{1}{n} \times \ln C_e \quad (13)$$

The values of the constants K_F and 1/n were determined from the curve ln q_e as a function of ln C_e.

Error calculation: To determine the model that best describes the adsorption of indigo carmine in synthetic and aqueous solution, error calculations involving the chi-square test (χ^2) and the sum of squared errors (SSE) were carried out. Eqns. 14 and 15 show, respectively, the formulas for χ^2 and SSE [27]:

$$\chi^2 = \sum_{i=1}^{n} \frac{(q_{e,exp} - q_{e,cal})^2}{q_{e,cal}} \quad (14)$$

$$SSE = \sum_{i=1}^{n} (q_{e,exp} - q_{e,cal})^2 \quad (15)$$

where $q_{e,exp}$ and $q_{e,cal}$ are the experimental and predicted adsorption capacities at equilibrium time, respectively.

RESULTS AND DISCUSSION

Morphology: Fig. 1 shows the morphological results for the corncob charcoal (Fig. 1a) and the iron oxide-charcoal composite (α-Fe_2O_3-C) (Fig. 1b). The SEM image of the charcoal revealed the presence of surface pores, whereas the iron oxide–charcoal composite exhibited a ruffled structure with large aggregates, indicating the incorporation of iron oxide particles into the charcoal. The pores observed on the corncob charcoal surface were attributed to the evaporation of water and volatile compounds during carbonization [31]. The iron oxide particles occupied these surface cavities, resulting in the rough morphology of the composite. This increased surface roughness provided favourable conditions for enhanced adsorption of pollutants, as reported earlier [32].

XRD studies: Fig. 2 presents the X-ray diffraction (XRD) patterns of the synthesized corn cob-iron oxide composite. Diffraction peaks appeared at 2θ values of 24.14º, 28.4º, 33.15º, 35.61º, 40.85º, 49.48º, 54.08º, 57.42º, 62.44º and 63.98º, corresponding to the (012), (104), (110), (113), (024), (116), (122), and (300) planes. Two intense peaks were observed at 33.15º (104) and 35.61º (110), while a smaller peak appeared at 28.4º. The average particle size of the composite, calculated using the Debye–Scherrer equation, was 20.63 nm. The XRD peaks confirmed the formation of hematite (α-Fe_2O_3) according to JCPDS card no. 33-0664 [8], with the intense peaks at 33.15º and 35.61º indicating its crystalline nature. The measured particle size further confirmed the nanometric character of the composite, consistent with the nanoparticle size range of 1-100 nm [33]. Furthermore, the peak at 28.4º corresponded to carbon derived from corncob charcoal [34], confirming the successful synthesis of the α-Fe_2O_3-C composite.

FTIR studies: Fig. 3 presents the Fourier Transform Infrared (FTIR) spectra of the composite (a) and corncob charcoal (b). A peak specific to the composite was observed at 814 cm^{-1}, while peaks specific to the charcoal appeared at 1580 and 2990 cm^{-1}. Both materials exhibited common peaks at 1060, 2030, 2190, 2580 and 3340 cm^{-1}, with the band at 3340 cm^{-1} broader in the composite than in the charcoal. For the charcoal, the band at 2990 cm^{-1} corresponded to the asymmetric C–H stretching vibration of methyl groups [35], while the 1580 cm^{-1} band was attributed to C=C stretching in aromatic rings. The the 900–410 cm^{-1} region represents the characteristic Fe–O vibrations [36]; thus, the peak at 814 cm^{-1} in the α-Fe_2O_3-C composite confirmed the presence of Fe–O

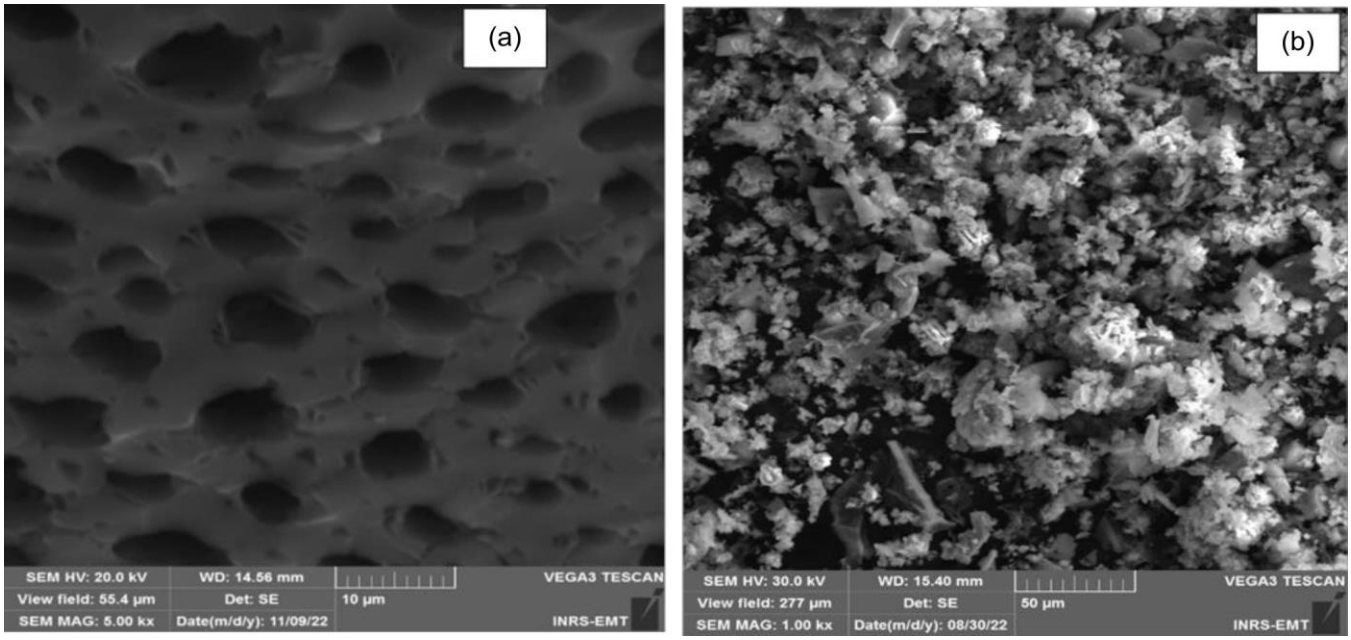

Fig. 1. SEM image of corn cob charcoal (a) and iron oxide-charcoal composite (b)

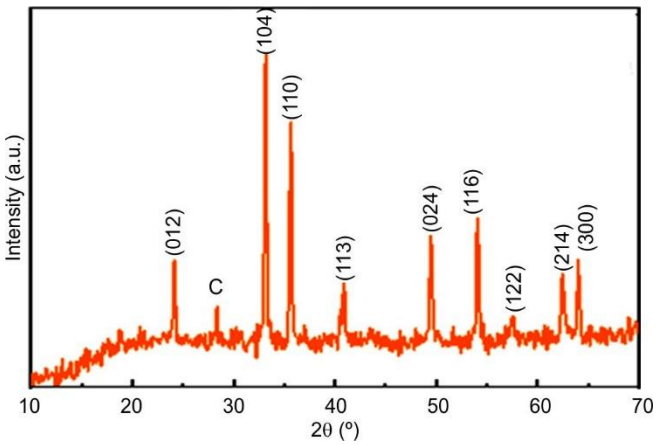

Fig. 2. X-ray diffractogram of the iron oxide-carbon composite

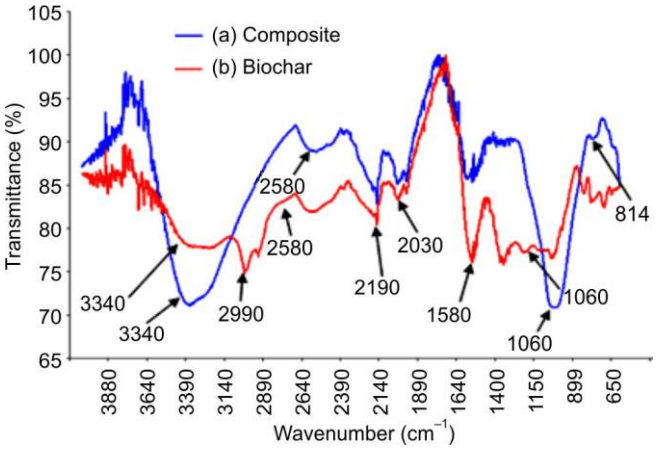

Fig. 3. Fourier transform infrared (FTIR) spectra of composite (a) and charcoal corncobs (b)

bonds. These FTIR results were consistent with the XRD analysis. The bands at 3340 cm^{-1} were assigned to the O–H stretching vibrations of phenolic, carboxylic or alcoholic groups [37] and the broadening in the α-Fe_2O_3-C composite likely reflected interactions between the carbon and iron oxide. The intense peaks at 1060 cm^{-1} are attributed to C–O stretching of ether groups on both charcoal and the composite [38], while the bands at 2190 and 2580 cm^{-1} corresponded to C=C vibrations of aromatic rings [39]. The presence of hydroxyl, carboxylic, phenolic and alcoholic groups on the α-Fe_2O_3-C surface is expected to enhance its adsorption capacity.

Thermogravimetric analysis (TGA): Fig. 4 shows the TGA results of the α-Fe_2O_3-C composite. Two stages of mass loss were observed. The first, a 1.5% loss between 25 ºC and 130 ºC, was attributed to the evaporation of water molecules adsorbed during synthesis [40]. In the second stage, a 20.5% loss between 350 ºC and 400 ºC, corresponded to the degradation of carbonaceous material in the composite [41]. Total

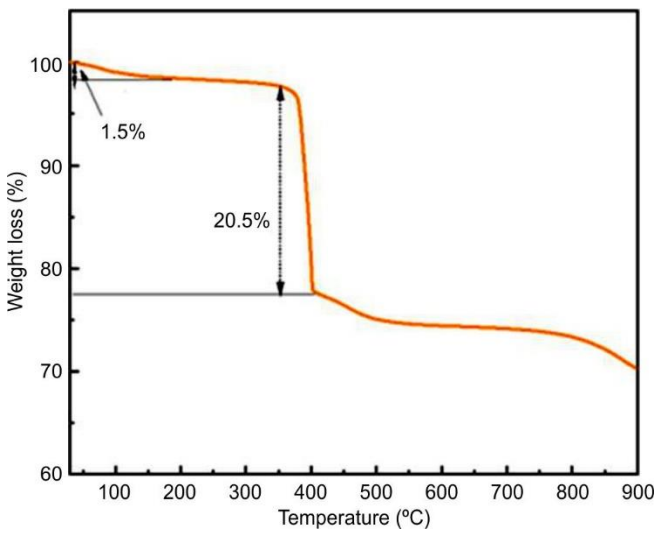

Fig. 4. Thermogravimetric analysis curve for α-Fe_2O_3-Charbon

mass loss was 22%, with further decrease observed above 400 ºC due to the gradual transformation of Fe_2O_3 into Fe [16,42]. The composite was stable up to 350 ºC and the TGA results indicate that it is predominantly composed of Fe_2O_3. These findings corroborated the XRD and FTIR analyses.

Magnetic properties: Fig. 5 illustrates the interaction of a bar magnet with the prepared corn-based composite. The attachment of the α-Fe_2O_3-C composite material to the magnet confirmed its magnetic properties, attributable to the presence of hematite (α-Fe_2O_3). These magnetic properties facilitate the separation of the composite from solution after indigo adsorption. Similar observations were reported by Liang *et al*. [43] and Oyekanmi *et al*. [44], who synthesized α-Fe_2O_3-charcoal composites with strong magnetic behaviour due to hematite, supporting the results of the present study.

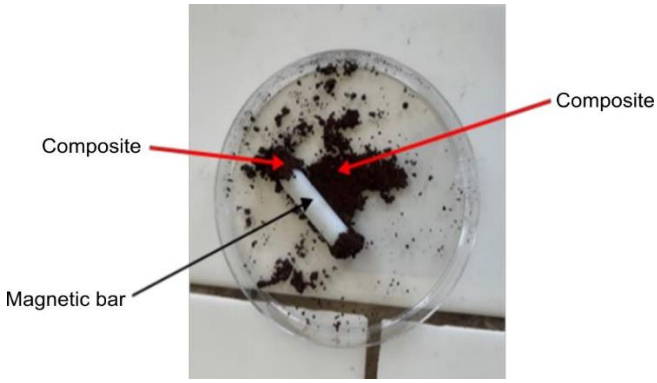

Fig. 5. Action of a bar magnetic on the composite

Adsorption studies of indigo carmine by biochar from corncob waste and its magnetic composite (α-Fe_2O_3-C)

Effect of contact time: Fig. 6 shows the time-dependent behaviour of indigo adsorption in both aqueous solution and textile effluent. Using charcoal (Fig. 6a), a rapid adsorption phase was observed, lasting from 0 to 15 min in aqueous solution and from 0 to 20 min in effluent. This is followed by a slower adsorption phase, spanning 15-35 min for aqueous solution and 20-90 min for effluent, until equilibrium is reached at 35 min and 90 min, respectively. For the composite (Fig. 6b), adsorption increases rapidly from 0 to 15 min in aqueous solution and from 0 to 35 min in effluent, followed by slower growth between 15-35 min and 35-90 min, respectively, before reaching equilibrium at the same times as above.

Adsorption percentages in aqueous solution range from 71.94% to 79.93% for carbon and 88.58% to 96.66% for the composite, whereas in textile effluent they vary from 31.74% to 43.66% for carbon and 48.01% to 61.90% for the α-Fe_2O_3-C composite. In both media, adsorption is higher in aqueous solution than in effluent. Moreover, as seen in Fig. 6c-d, the composite consistently achieves higher adsorption rates than carbon. The initial rapid adsorption is attributed to the abundance of available sites on the adsorbent [8], while the subsequent slower phase corresponds to the gradual occupation of

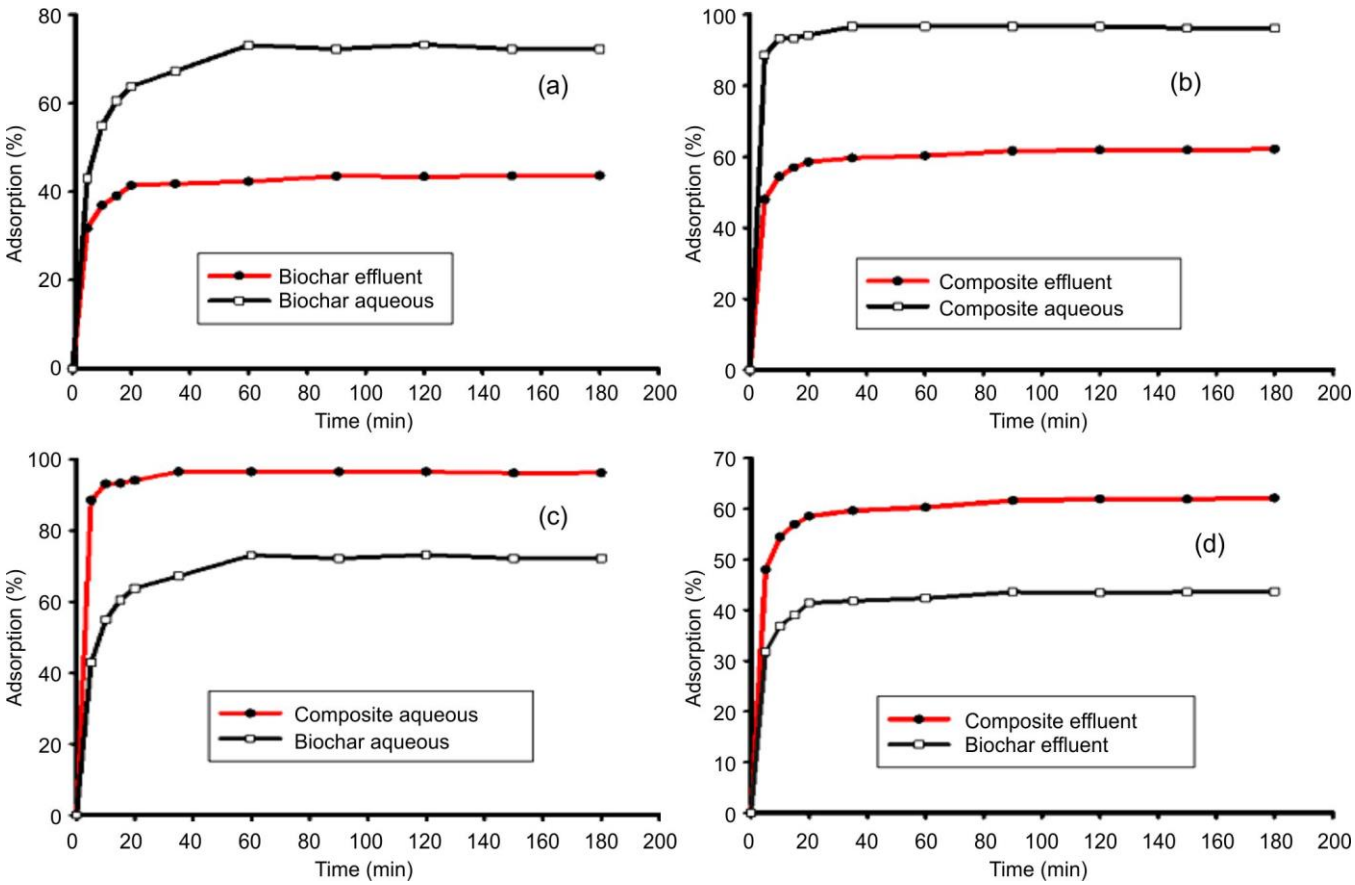

Fig. 6. Percentage adsorption of indigo carmine in aqueous solution and textile effluent

these sites [27]. Equilibrium is reached when the accessible sites at the solid-liquid interface are saturated. The lower adsorption observed in effluent is likely due to blockage of active sites by other pollutants [27]. Similar findings were reported by El-Kammah *et al.* [45] using moringa seeds for indigo removal from textile effluents in Egypt. The superior performance of the α-Fe_2O_3-C composite suggests that coupling carbon with iron oxide creates additional active sites, making it an effective adsorbent for both aqueous and real solutions.

Kinetic studies: The pseudo-second-order model exhibits coefficients of determination (R^2) between 0.982 and 0.998, indicating excellent fit, while the pseudo-first-order model shows lower R^2 values ranging from 0.765 to 0.982 (Figs. 7 and 8). The error values for the pseudo-second-order model are 2.99×10^{-4} to 6.7×10^{-4} for χ^2 and 1.8×10^{-4} to 6.52×10^{-4} for SSE. Corresponding errors for the pseudo-first-order model are 26.845-70.773 (χ^2) and 1.242-6.943 (SSE). The theoretical maximum adsorption capacities (Qe_2 theort.) from the pseudo-second-order model range from 0.449 mg/g to 0.978 mg/g, compared to 0.086–0.130 mg/g (Qe_1 theort.) for the pseudo-first-order model. Experimentally, carbon achieves Q_{exp} values of 0.798 mg/g (aqueous solution) and 0.441 mg/g (effluent), while the composite reaches 0.961 mg/g and 0.616 mg/g, respectively. Overall, the pseudo-second-order model better describes indigo carmine adsorption behaviour, as indicated by higher R^2 values, lower χ^2 and SSE errors and close agreement between the theoretical and experimental Q_e values (Table-1). This suggests chemisorption as the dominant mechanism, consistent with findings by Nascimento *et al.* [46] for Fe_3O_4-sugarcane straw composites.

Adsorption isotherms: Fig. 9a demonstrates that increasing initial indigo carmine concentration also increases the removal percentages, ranging from 76.83% to 88.55% for the composite and 32.84% to 49.22% for carbon, with maximum removal at 5 mg/L. The composite consistently outperforms carbon. Fig. 9b shows that the equilibrium adsorption amount (Q_e) increases with residual indigo concentration (C_e), with higher adsorption for the composite.

Adsorption isotherms (Fig. 10, Table-2) indicate that the Langmuir model best fits the composite ($R^2 = 0.9980$), while the Freundlich model better represents charcoal ($R^2 = 0.9803$ *vs.* 0.975). Maximum adsorption capacities were found to be 4.76 mg/g (charcoal) and 12.72 mg/g (composite). Reduced adsorption at higher indigo concentrations is attributed to the saturation of active sites [27]. Similar trends were reported by Odugu *et al*. [47] and Davies & McGregor [48] also observed increases in adsorption with higher initial concentrations.

Freundlich constants n >1 indicate favorable adsorption, and positive Langmuir constants suggest spontaneous adsorption at room temperature. Comparing Q_m values, the composite in this study (12.72 mg/g) is lower than Ce-MOF-Fe_3O_4-activated carbon (85.5 mg/g) [49], $MnFe_2O_4$-moringa seed activated carbon (33.53 mg/g) [50], and Fe_3O_4-avocado kernel activated carbon (49 mg/g) [48], but higher than Fe_3O_4-sugarcane straw (1.46 mg/g) [46], Fe_3O_4-banana peelings (8.72 mg/g) [51] and $MnFe_2O_4$-wood sawdust (1.74 mg/g) [52].

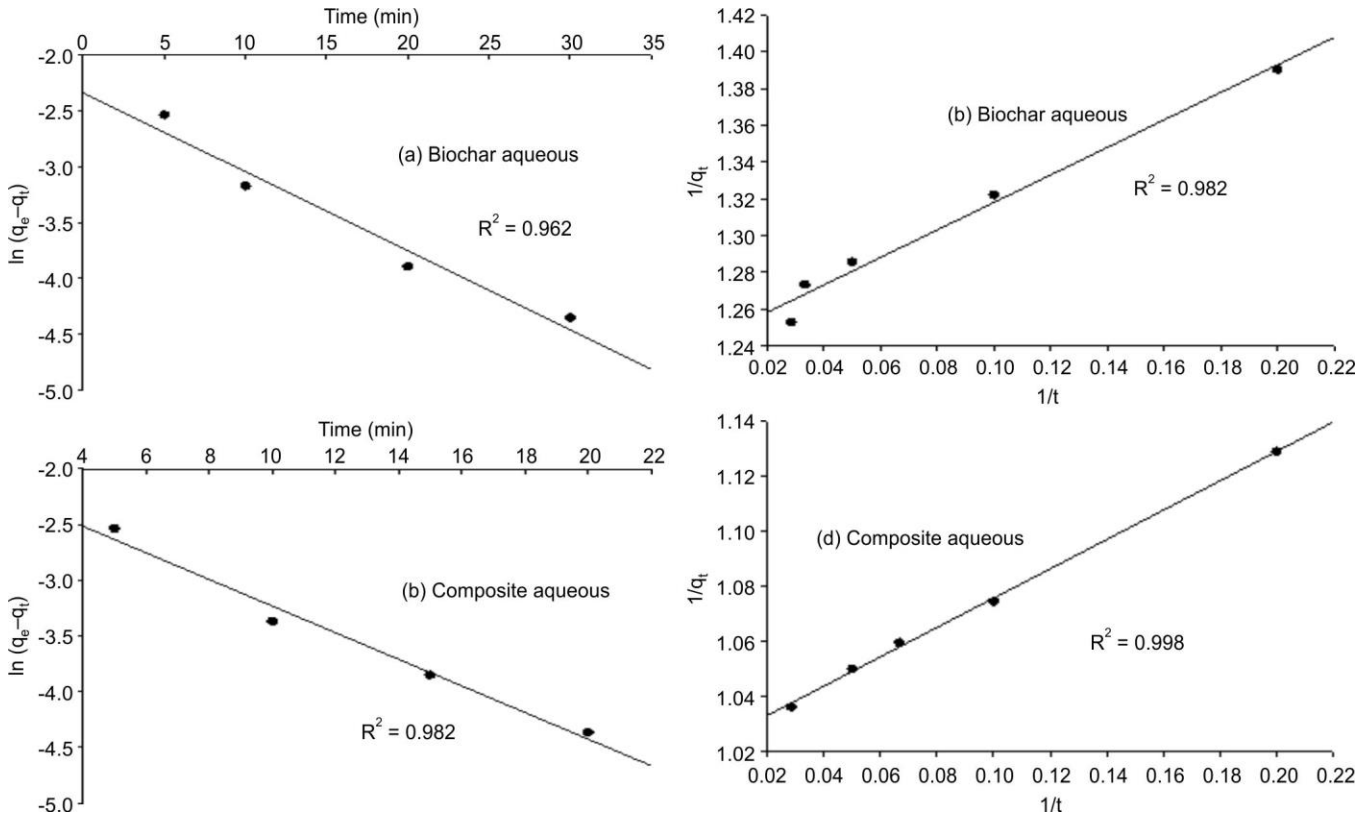

Fig. 7. Linear representations of the pseudo-first-order (a,c) and pseudo-second-order (b,d) kinetic model of indigo adsorption in aqueous solution

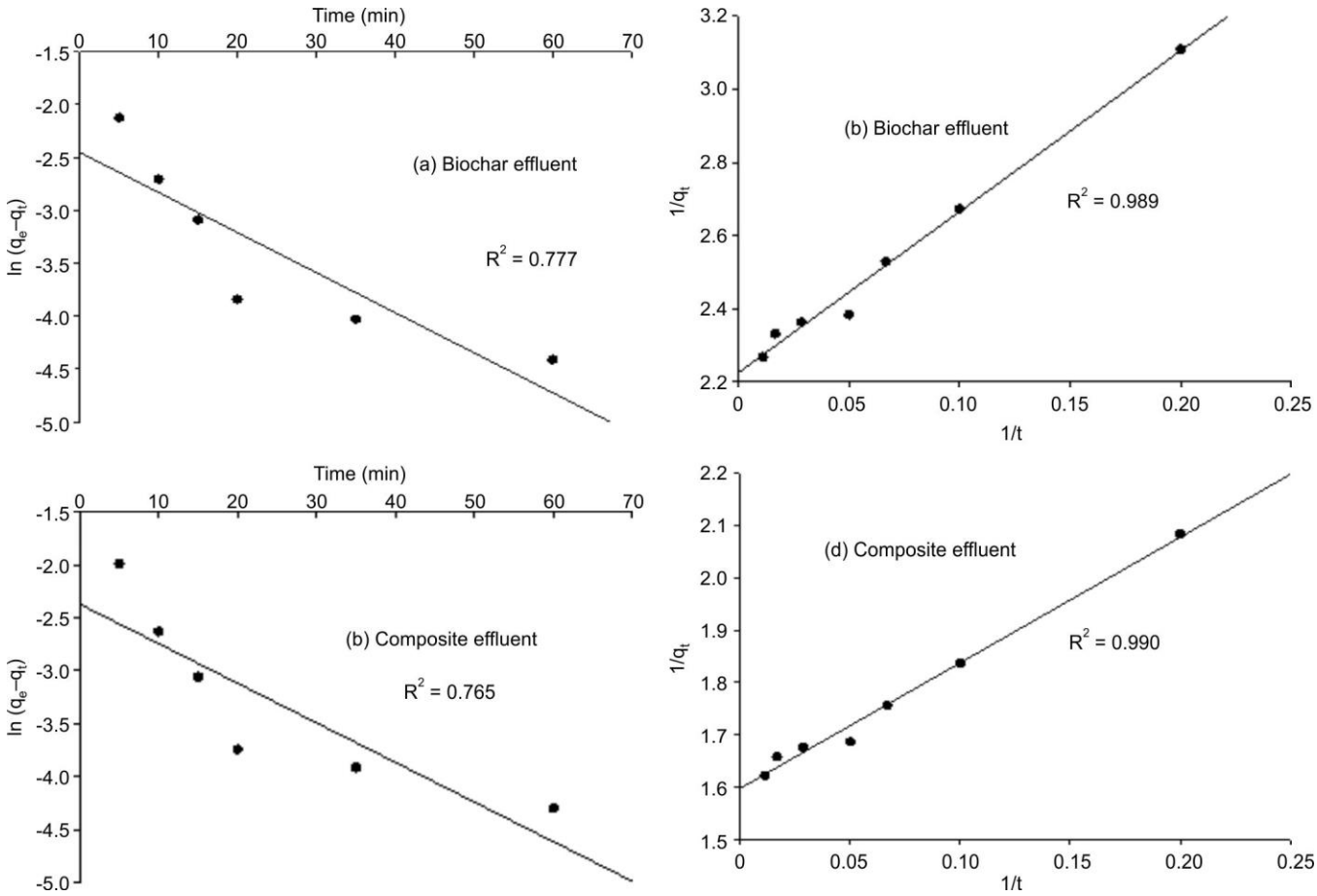

Fig. 8. Linear representations of the pseudo-first-order (a,c) and pseudo-second-order (b,d) kinetic model of indigo adsorption in effluent

TABLE-1
CONSTANTS FOR PSEUDO-FIRST-ORDER AND PSEUDO-SECOND-ORDER KINETIC MODELS

Biochar	Aqueous solution: 0.798		Effluent: 0.441	
Composite (α-Fe_2O_3@C)	Aqueous solution: 0.965		Effluent: 0.616	
Model		Aqueous solution		Effluent
		Biochar	Composite	Biochar	Composite
Pseudo first order	Qe_1 (mg/g)	0.096	0.130	0.086	0.094
	k_1	0.071	0.120	0.038	0.037
	χ^2	70.773	63.827	26.845	54.955
	SSE	4.913	6.943	1.242	2.712
	R^2	0.962	0.982	0.777	0.765
Pseudo second order	Qe_2 (mg/g)	0.804	0.978	0.449	0.626
	k_2	2.088	1.964	1.126	1.067
	χ^2	2.99×10^{-4}	6.7×10^{-4}	4.2×10^{-4}	3.19×10^{-4}
	SSE	2.37×10^{-4}	6.52×10^{-4}	1.8×10^{-4}	1.89×10^{-4}
	R^2	0.982	0.998	0.989	0.990

Effect of adsorbent mass: Fig. 11 shows that increasing adsorbent mass from 0.1 g to 0.3 g improves the adsorption from 10.97% to 73.91% for carbon and 52.37% to 97.43% for the composite. Beyond 0.3 g, adsorption decreases, likely due to site saturation [25]. The optimal composite mass for effective effluent treatment is therefore 0.3 g.

Conclusion

This study focuses on the removal of indigo carmine from wastewater through adsorption using a novel adsorbent based on corncob-based iron oxide-carbon (α-Fe_2O_3-C) composite. XRD analysis confirmed the formation of an α-Fe_2O_3-C composite with an average particle size of 20.63 nm. FTIR results revealed the presence of carboxylic, hydroxyl, phenolic and alcoholic func-tional groups on the composite surface indicating that Fe_2O_3 is the predominant phase in the material. Kinetic studies showed that the composite achieved higher adsorption percentages than carbon in both aqueous solution (88.58-96.66% for the composite and 71.94-79.93% for biochar corncob) and real textile effluent (48.01-61.90% for

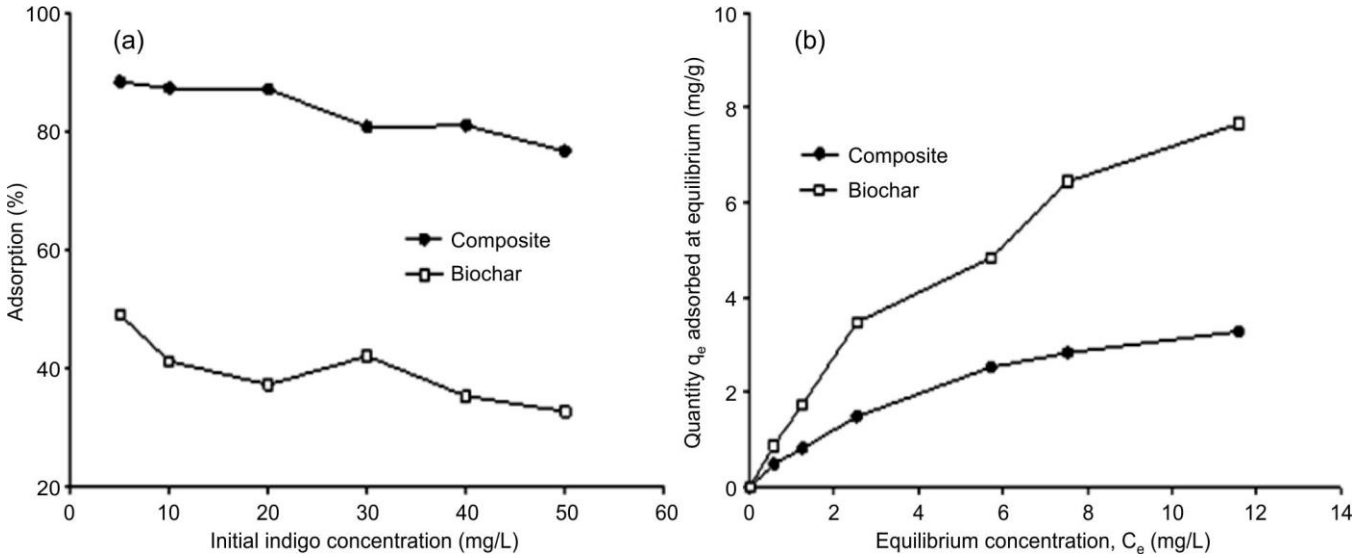

Fig. 9. Percentage of indigo adsorption as a function of initial indigo concentration (a) and indigo adsorption isotherms (b)

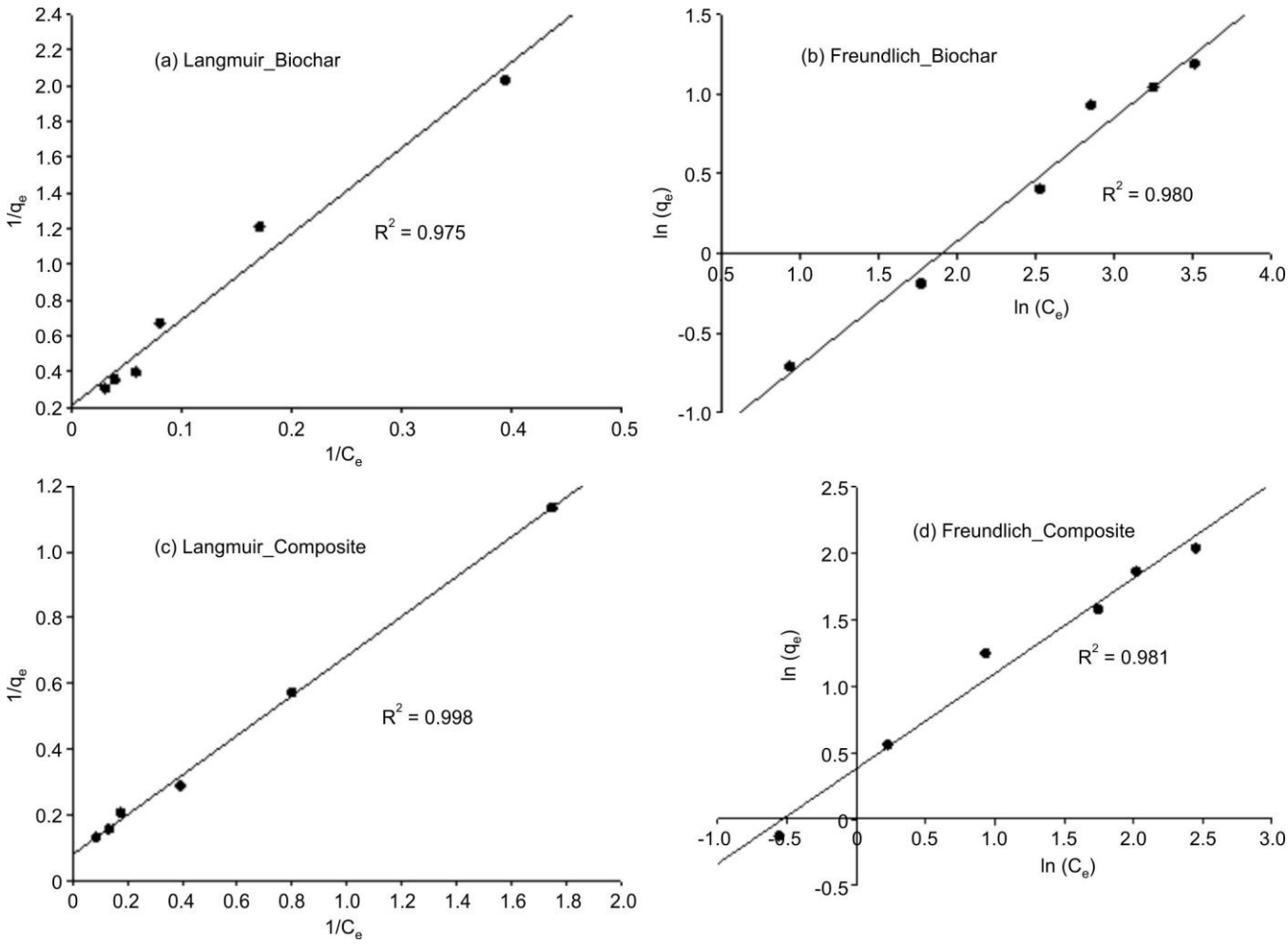

Fig. 10. Linear representations of Langmuir (a,c) and Freundlich (b,d) models

the composite and 31.74-43.66% for carbon), confirming that α-Fe_2O_3-C significantly enhances indigo carmine adsorption. Adsorption kinetics were best described by the pseudo-second-order model, suggesting chemisorption as the main mechanism. In aqueous solution, the initial indigo carmine concentration influenced adsorption efficiency, with maximum removal observed at 5 mg/L for both adsorbents: 49.22% for carbon and 88.55% for the composite. Adsorption isotherm analysis indicated that the Freundlich model best describes indigo carmine adsorption on charcoal (R^2 = 0.9803), whereas the

TABLE-2
LANGMUIR AND FREUNDLICH MODEL CONSTANTS

Models	Parameter	Values	
		Biochar	Composite
Langmuir	Q_{max} (mg/g)	4.76	12.72
	K_L	0.043	0.13
	R^2	0.975	0.998
	χ^2	0.281	0.099
	SSE	0.625	0.465
Freundlich	K_F	0.229	1.46
	N	1.291	1.39
	R^2	0.980	0.981
	χ^2	0.123	0.252
	SSE	0.260	1.233

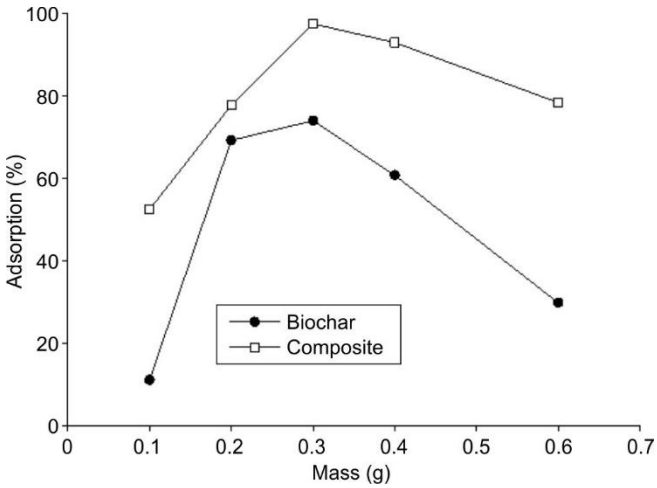

Fig. 11. Mass effect on indigo adsorption in textile effluent

Langmuir model provides a better fit for the α-Fe_2O_3-C composite (R^2 = 0.9980). The corresponding maximum adsorption capacities were 4.76 mg/g for carbon and 12.72 mg/g for the α-Fe_2O_3-C composite. The effect of adsorbent mass on indigo carmine removal from textile effluent revealed that 0.3 g was found to be optimal for both adsorbents, achieving maximum removal of 73.91% for carbon and 97.43% for the composite.

ACKNOWLEDGEMENTS

The authors gratefully acknowledge the institutions that provided the research materials essential for this study.

CONFLICT OF INTEREST

The authors declare that there is no conflict of interests regarding the publication of this article.

REFERENCES

1. M. Ismail, K. Akhtar, M.I. Khan, T. Kamal, M.A. Khan, A. M. Asiri, J. Seo and S.B. Khan, *Curr. Pharm. Des.*, **25**, 3645 (2019); https://doi.org/10.2174/1381612825666191021142026
2. R. Al-Tohamy, S.S. Ali, F. Li, K.M. Okasha, Y.A.-G. Mahmoud, T. Elsamahy, H. Jiao, Y. Fu and J. Sun, *Ecotoxicol. Environ. Saf.*, **231**, 113160 (2022); https://doi.org/10.1016/j.ecoenv.2021.113160
3. T.S. Algarni and A.M. Al-Mohaimeed, *J. King Saud Univ. Sci.*, **34**, 102339 (2022); https://doi.org/10.1016/j.jksus.2022.102339
4. M.F. Chowdhury, S. Khandaker, F. Sarker, A. Islam, T.M. Rahman and M.R. Awual, *J. Mol. Liq.*, **318**, 114061 (2020); https://doi.org/10.1016/j.molliq.2020.114061
5. A.N. Babu, D.S. Reddy, P. Sharma, G.S. Kumar, K. Ravindhranath and G.V.K. Mohan, *Mater. Today Proc.*, **17**, 198 (2019); https://doi.org/10.1016/j.matpr.2019.06.419
6. S. Ben Salah, M. Missaoui, A. Attia, G. Lesage, M. Heran and R. Ben Amar, *Front. Membr. Sci. Technol.*, **3**, 1348992. (2024); https://doi.org/10.3389/frmst.2024.1348992
7. S.N. Eroi, A.S. Ello, D. Diabaté and D.B. Ossonon, *S. Afr. J. Chem. Eng.*, **3**, 53 (2021); https://doi.org/10.1016/j.sajce.2021.03.009
8. S. Somma, E. Reverchon and L. Baldino, *ChemEngineering*, **5**, 47 (2021); https://doi.org/10.3390/chemengineering5030047
9. M. Munoz, J. Nieto-Sandoval, S. Álvarez-Torrellas, E. Sanz-Santos, B. Calderón, Z.M. de Pedro, M. Larriba, A. Fullana, J. García and J.A. Casas, *Sep. Purif. Technol.*, **257**, 117974 (2021); https://doi.org/10.1016/j.seppur.2020.117974
10. J. Ku, K. Wang, Q. Wang and Z. Lei, *Separations*, **11**, 130 (2024); https://doi.org/10.3390/separations11050130
11. N. Ghosh, S. Sen, G. Biswas, A. Saxena and P.K. Haldar, *Water Air Soil Pollut.*, **234**, 202 (2023); https://doi.org/10.1007/s11270-023-06217-8
12. I. Ashraf, N.B. Singh and A. Agarwal, *Mater. Today Proc.*, **72**, 311 (2023); https://doi.org/10.1016/j.matpr.2022.07.404
13. S. Bhukal, A. Sharma, Rishi, Divya, S. Kumar, B. Deepak, K. Pal and S. Mona, *Top. Catal.*, **65**, 1675 (2022); https://doi.org/10.1007/s11244-022-01640-3
14. L.M. Mahlaule-Glory, S. Mapetla, A. Makofane, M.M. Mathipa and N.C. Hintsho-Mbita, *Heliyon*, **8**, e10536 (2022); https://doi.org/10.1016/j.heliyon.2022.e10536
15. M. Haris, A. Zavabeti, M.W. Khan, B.J. Murdoch, J. Paz-Ferreiro, N. Mahmood and N. Eshtiaghi, *J. Environ. Chem. Eng.*, **10**, 108968 (2022); https://doi.org/10.1016/j.jece.2022.108968
16. Y. Qiu, X. Xu, Z. Xu, J. Liang, Y. Yu and X. Cao, *Chem. Eng. J.*, **389**, 124471 (2020); https://doi.org/10.1016/j.cej.2020.124471
17. J. Xie, R. Lin, Z. Liang, Z. Zhao, C. Yang and F. Cui, *J. Environ. Chem. Eng.*, **9**, 105744 (2021); https://doi.org/10.1016/j.jece.2021.105744
18. O.I. Ali, E.R. Zaki, M.S. Abdalla and S.M. Ahmed, *Environ. Sci. Pollut. Res. Int.*, **30**, 53548 (2023); https://doi.org/10.1007/s11356-023-26000-w
19. Y. Zhou, S. Cao, C. Xi, X. Li, L. Zhang, G. Wang and Z. Chen, *Bioresour. Technol.*, **292**, 121951 (2019); https://doi.org/10.1016/j.biortech.2019.121951
20. Y. Kanchanaroek, T. Rattanakaew, P. Kako, O. Meangbua and W. Doungjun, *Sustain. Environ. Res.*, **35**, 23 (2025); https://doi.org/10.1186/s42834-025-00261-1
21. R.P. Na Talang, W. Na Sorn, S. Polruang and S. Sirivithayapakorn, *Sci. Rep.*, **14**, 14372 (2024); https://doi.org/10.1038/s41598-024-65389-3
22. K.N. Aboua, Y.A. Yobouet, K.B. Yao, D.L. Goné and A. Trokourey, *J. Environ. Manage.*, **156**, 10 (2015); https://doi.org/10.1016/j.jenvman.2015.03.006
23. U.Y. Kouakou, A. Dembélé, A.Y. Yobouet and A. Trokourey, *Int. J. Adv. Res. Sci. Eng. Technol.*, **3**, 2573 (2016).
24. P.H.K. Ouattara, M.I. Gouli, U. Kouakou, A. Dembélé, J.Y. Aboua and A. Trokourey, *Int. J. Sci. Res.*, **3**, 933 (2014).
25. K.P.A. N'goran, D. Diabaté, K.M. Yao, N.L.B. Kouassi, U.P. Gnonsoro, K.C. Kinimo and A. Trokourey, *Arab. J. Geosci.*, **11**, 498 (2018); https://doi.org/10.1007/s12517-018-3862-2
26. A.F. Kokora, L.D. Kouadio, D.B. Soro, K.R. N'guettia, A. Dembélé and K.S. Traoré, *Rev. Ivoir. Sci. Technol.*, **31**, 39 (2018).
27. N.L.B. Kouassi, K.P.D.A. N'goran, L.D. Blonde, D. Diabate and T. Albert, *Chem. Afr.*, **6**, 733 (2023); https://doi.org/10.1007/s42250-022-00432-2
28. Y. Ma, M. Li, P. Li, L. Yang, L. Wu, F. Gao, X. Qi and Z. Zhang, *Bioresour. Technol.*, **319**, 124199 (2021); https://doi.org/10.1016/j.biortech.2020.124199

29. S. Lagergren, *K. Sven. Vetensk. Akad. Handl.*, **24**, 1 (1898).
30. Y.S. Ho and G. McKay, *Process Biochem.*, **34**, 451 (1999); https://doi.org/10.1016/S0032-9592(98)00112-5
31. S.A. Dhar, T.U. Sakib and L.N. Hilary, *Biomass Convers. Biorefin.*, **12**, 2631 (2022); https://doi.org/10.1007/s13399-020-01116-y
32. J. Fito, M. Abewaa and T. Nkambule, *Appl. Water Sci.*, **13**, 78 (2023); https://doi.org/10.1007/s13201-023-01880-y
33. T.D. Piluk, G. Faccio, S. Letsiou, R. Liang and M. Freire-Gormaly, *Environ. Sci. Nano*, **11**, 3674 (2024); https://doi.org/10.1039/D4EN00489B
34. V. Ranjithkumar, S. Sangeetha and S. Vairam, *J. Hazard. Mater.*, **273**, 127 (2014); https://doi.org/10.1016/j.jhazmat.2014.03.034
35. J. Xu, Y. Liu, J. He, R. Zhang, B. Zuo, and X. Wang, *Soft Matter*, **10**, 8992 (2014); https://doi.org/10.1039/C4SM01743A
36. D. Flores-Cano, N.R. Checca-Huaman, I.L. Castro-Merino, C.N. Pinotti, E.C. Passamani, J.F. Litterst and J.A. Ramos-Guivar, *Int. J. Mol. Sci.*, **23**, 8279 (2022); https://doi.org/10.3390/ijms23158279
37. J.A.A. Abdullah, L. Salah Eddine, B. Abderrhmane, M. Alonso-González, A. Guerrero and A. Romero, *Sustain. Chem. Pharm.*, **17**, 100280 (2020); https://doi.org/10.1016/j.scp.2020.100280
38. D. Bhatia, D. Datta, A. Joshi, S. Gupta and Y. Gote, *J. Mol. Liq.*, **276**, 163 (2019); https://doi.org/10.1016/j.molliq.2018.11.127
39. M. Jain, M. Yadav, T. Kohout, M. Lahtinen, V.K. Garg and M. Sillanpää, *Water Resour. Ind.*, **20**, 54 (2018); https://doi.org/10.1016/j.wri.2018.10.001
40. Y. Xiong, F. Ye, C. Zhang, S. Shen, L. Su and S. Zhao, *RSC Adv.*, **5**, 5164 (2015); https://doi.org/10.1039/C4RA12468E
41. E.R. Monazam, R.W. Breault and R. Siriwardane, *Chem. Eng. J.*, **242**, 204 (2014); https://doi.org/10.1016/j.cej.2013.12.040
42. M. Jayashree, M. Parthibavarman and S. Prabhakaran, *Ionics*, **25**, 3309 (2019); https://doi.org/10.1007/s11581-019-02859-z
43. H. Liang, C. Zhu, S. Ji, P. Kannan and F. Chen, *Biochar*, **4**, 3 (2022); https://doi.org/10.1007/s42773-021-00130-1
44. A.A. Oyekanmi, K.K. Katibi, R.C. Omar, A. Ahmad, M. Elbidi, M.B. Alshammari and H.G. Shitu, *Appl. Water Sci.*, **14**, 13 (2024); https://doi.org/10.1007/s13201-023-02060-8
45. M. El-Kammah, E. Elkhatib, S. Gouveia, C. Cameselle and E. Aboukil, *Environ. Technol. Innov.*, **28**, 102 (2022); https://doi.org/10.1016/j.eti.2022.102713
46. R.K. do Nascimento, B.S. Damasceno, A.N. de Melo, P.H.M. de Farias, J.V.F.L. Cavalcanti, D.C.S. Sales, E.H.L. Falcão and A.C.V. de Araújo, *Cellulose*, **30**, 2483 (2023); https://doi.org/10.1007/s10570-022-04978-9
47. A.N. Odogu, D. Kouotou, L.P. Keilah, A.T. Godwin, N.R. Lekene, J.N. Nsami and J.M. Ketcha, *Arab. J. Chem.*, **13**, pp5241 (2020); https://doi.org/10.1016/j.arabjc.2020.03.002
48. G. Davies and J. McGregor, *ACS Omega*, **6**, 33000 (2021); https://doi.org/10.1021/acsomega.1c05116
49. R. Paz, H. Viltres, N.K. Gupta and C. Leyva, *J. Mol. Liq.*, **337**, 116578 (2021); https://doi.org/10.1016/j.molliq.2021.116578
50. P. Sirajudheen, P. Karthikeyan, P. Ramkumar, P. Nisheetha and S. Meenakshi, *J. Mol. Liq.*, **327**, 114829 (2021); https://doi.org/10.1016/j.molliq.2020.114829
51. D. Channei, K. Chansaenpak, P. Jannoey, W. Khanitchaidecha, H. Sintuya, A. Nakarukg and S. Phanichphant, *Desalination Water Treat.*, **225**, 340 (2021).
52. S. Hashemian and M. Hidarian, *Orient. J. Chem.*, **30**, 1753 (2014); https://doi.org/10.13005/ojc/300434